High-performance intrinsically microporous dihydroxyl-functionalized triptycene-based polyimide for natural gas separation

Accepted Manuscript

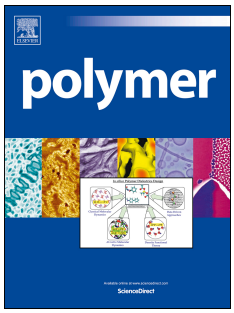

High-performance intrinsically microporous dihydroxyl-functionalized triptycene-based polyimide for natural gas separation

Nasser Alaslai, Bader Ghanem, Fahd Alghunaimi, Ingo Pinnau

PII: S0032-3861(16)30209-9

DOI: 10.1016/j.polymer.2016.03.063

Reference: JPOL 18555

To appear in: *Polymer*

Received Date: 18 February 2016

Revised Date: 14 March 2016

Accepted Date: 20 March 2016

Please cite this article as: Alaslai N, Ghanem B, Alghunaimi F, Pinnau I, High-performance intrinsically microporous dihydroxyl-functionalized triptycene-based polyimide for natural gas separation, *Polymer* (2016), doi: 10.1016/j.polymer.2016.03.063.

High-performance intrinsically microporous dihydroxyl-functionalized triptycene-based polyimide for natural gas separation

Nasser Alaslai, Bader Ghanem, Fahd Alghunaimi, Ingo Pinnau*

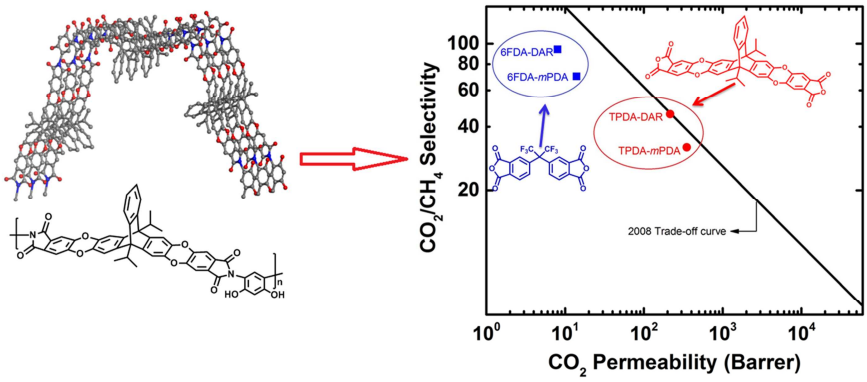

High-performance intrinsically microporous dihydroxyl-functionalized triptycene-based polyimide for natural gas separation

Nasser Alaslai, Bader Ghanem, Fahd Alghunaimi, Ingo Pinnau*

[*]*King Abdullah University of Science and Technology (KAUST), Advanced Membranes and Porous Materials Center (AMPMC), Division of Physical Sciences and Engineering, Chemical and Biological Engineering Program, Thuwal 23955-6900, Saudi Arabia*

*Corresponding author: King Abdullah University of Science and Technology, Advanced Membranes and Porous Materials Center, Division of Physical Sciences and Engineering Al-Jazri Bldg. 4, Thuwal 23955-6900, Saudi Arabia, Tel: +966-12-808-2406

E-mail address: ingo.pinnau@kaust.edu.sa (I. Pinnau)

Abstract

A novel polyimide of intrinsic microporosity (PIM-PI) was synthesized from a 9,10-diisopropyl-triptycene-based dianhydride (TPDA) and dihydroxyl-functionalized 4,6-diaminoresorcinol (DAR). The unfunctionalized TPDA-*m*-phenylenediamine (*m*PDA) polyimide derivative was made as a reference material to evaluate the effect of the OH group in TPDA-DAR on its gas transport properties. Pure-gas permeability coefficients of He, H_2, N_2, O_2, CH_4, and CO_2 were measured at 35 °C and 2 atm. The BET surface area based on nitrogen adsorption of dihydroxyl-functionalized TPDA-DAR (308 m^2g^{-1}) was 45% lower than that of TPDA-*m*PDA (565 m^2g^{-1}). TPDA-*m*PDA had a pure-gas CO_2 permeability of 349 Barrer and CO_2/CH_4 selectivity of 32. The dihydroxyl-functionalized TPDA-DAR polyimide exhibited enhanced pure-gas CO_2/CH_4 selectivity of 46 with a moderate decrease in CO_2 permeability to 215 Barrer. The CO_2 permeability of TPDA-DAR was ~30-fold higher than that of a commercial cellulose triacetate membrane coupled with 39% higher pure-gas CO_2/CH_4 selectivity. The TPDA-based dihydroxyl-containing polyimide showed good plasticization resistance and maintained high mixed-gas selectivity of 38 when tested at a typical CO_2 natural gas wellhead CO_2 partial pressure of 10 atm.

Keywords: triptycene polyimides, hydroxyl functionalization, mixed-gas permeation

Introduction

Membrane-based natural gas separation is a rapidly expanding technology, specifically for CO_2/CH_4 separation for natural gas and biogas treatment [1-7]. This application utilizes all of the potential advantages of membrane technology: (i) simple and continuous operation, (ii) no phase changes in the feed, (iii) environmentally benign separation process, (iv) small footprint (important for offshore systems) and (v) energy efficiency [3, 5]. Current large-scale membrane systems process up to 1 Bscfd using flat-sheet or hollow fiber cellulose acetate (CA) integrally-skinned asymmetric membranes [5, 8]. Baker and Lokhandwala showed that the process economics can be significantly improved with membrane materials that exhibit higher CO_2 permeability, and more importantly, higher CO_2/CH_4 mixed gas selectivity than CA [3]. The former reduces the size, and therefore the capital cost of the membrane system, whereas the latter leads to reduced methane loss which in many cases determines the overall economics of the membrane unit. Consequently, there is a quest for advanced membranes with high CO_2 permeability and high mixed-gas CO_2/CH_4 selectivity for high-pressure natural gas sweetening applications [9-11].

Designing and developing new membranes with improved gas separations properties requires rational molecular design of advanced polymeric materials [12, 13]. Enhanced gas separation performance can be achieved by introducing intrinsic micropores into highly rigid, glassy polymers that can improve gas permeability [12]. In 2004, the first ladder-type polymers of intrinsic microporosity (PIMs) were reported by Budd and McKeown [14, 15]. These PIMs are composed of structurally contorted backbones consisting of spiro-centers and fused dioxane rings resulting in inefficient packing of polymer chains. Ladder-type PIMs showed good gas separation performance because their molecular structures give rise to microporosity of less than 20 Å, combining high permeability with moderate selectivity for separation of O_2/N_2 and CO_2/N_2 [16-18]. Since then, many efforts have been devoted to improve the performance of ladder-type PIMs [19-27] and an early example was tetrazole-functionalized PIM-1 (TZPIM) that showed excellent CO_2 permeability and high CO_2/N_2 selectivity [26]. Other modifications of PIM-1 by post-treatment with functional groups include carboxyl, thioamide, amidoxime and thermal oxidative crosslinking [27-31].

Over the past 30 years, polyimides (PIs) have been investigated intensively as advanced gas separation membrane materials [32-37]. Previous work showed that hydroxyl-functionalized 6FDA-based polyimides exhibit some of the highest CO_2/CH_4 selectivities reported for all known polymeric materials to date [38-44]. However, the CO_2 permeability of these polyimides is relatively low (typically less than 10 Barrer).

In 2008, an effective integration of the ladder-type, kinked repeat unit characteristic of PIM-1 into polyimide structures (PIM-PI) has generated among the most permeable, intrinsically microporous polyimides with performance close to the 2008 upper bound for several important gas pairs [22, 23, 45]. However, the selectivities of these first generation PIM-PIs were too low to be commercially attractive. Recently, our group reported a series of 9,10-diisopropyltriptycene-based PIM-PIs known as KAUST PIs [46-48]. These polymers contain a bridged triptycene moiety that provides *rigidity* and *ultramicroporosity* (pore size < 7 Å) to their structure. KAUST PIs showed remarkable gas separation performance to levels that far exceeded the 2008 Robeson upper bounds with new limits set in recently reported 2015 trade-off curves for O_2/N_2, H_2/N_2, H_2/CH_4 [49, 50]. Unfortunately, although KAUST PIs exhibited very high CO_2 permeability their CO_2/CH_4 selectivity was lower than that of commercial membrane materials.

Here, we report the synthesis, structural characterization and pure- and mixed-gas permeation properties of a novel dihydroxyl-functionalized 9,10-diisopropyl-triptycene-dianhydride-based PIM-PI (TPDA-DAR in **Scheme 1**). In addition, to evaluate the effect of the hydroxyl-functionalization on the *m*-phenylenediamine polyimide building block, TPDA-*m*PDA was synthesized and characterized as a reference material. The PIM-PIs were fully characterized by ^{1}H NMR, FTIR, GPC (only for TPDA-*m*PDA), and TGA. Nitrogen and carbon dioxide adsorption experiments were performed to reveal the micropore structure of the PIM-PIs.

Experimental

Materials

Isoquinoline, benzoic acid and triethylamine (Et_3N) were obtained from Aldrich and used as received. *m*-Phenylenediamine (*m*PDA) was purchased from Aldrich and purified by sublimation under vacuum prior to use. 4,6-Diaminoresorcinol dihydrochloride (DAR) was received from Aldrich and dried under vacuum for 20 hours at room temperature. *m*-Cresol was purchased

from Aldrich and dried over 4 Å molecular sieves prior to use. All other solvents were obtained from various commercial sources and used as received.

Synthesis of the triptycene-based dianhydride (TPDA)

The triptycene-based tetracarboxylic dianhydride was prepared through a six-step synthetic route as previously reported by Ghanem et al. [47].

Synthesis of the polyimides

Two polyimides TPDA-*m*PDA and TPDA-DAR were synthesized *via* the cycloimidization reaction between equimolar amounts of the previously synthesized triptycene-based dianhydride (TPDA) and the corresponding diamine in *m*-cresol and, in the case of TPDA-DAR, in presence of triethylamine and benzoic acid as catalyst (**Scheme 1**). The polymers demonstrated good solubility in various organic solvents from which self-supporting and transparent flexible films were cast.

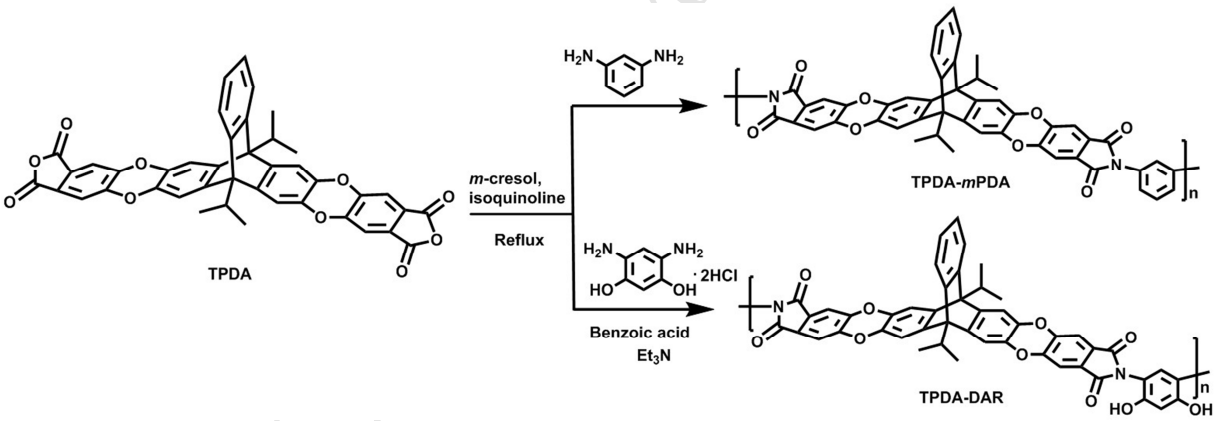

Scheme 1. Synthesis of TPDA-*m*PDA and TPDA-DAR polyimides.

Synthesis of TPDA-*m*PDA polyimide

Into a dry 10 mL Schlenk tube were added *m*-phenylenediamine (0.065 g, 0.6 mmol), TPDA (0.41 g, 0.6 mmol) and freshly distilled *m*-cresol (3 ml). After stirring for 30 minutes at ambient temperature and under a flow of nitrogen, catalytic amount of isoquinoline was added and the temperature was raised gradually to 200 °C and maintained at that temperature for 3 hours.

During the heating, water produced by the imidization reaction was removed with a stream of nitrogen. After cooling, the reaction mixture was added to methanol (200 ml) and the resulting fibrous polymer was purified from a chloroform/methanol mixture and then dried under vacuum at 130 °C for 20 h to give a white powder in 86% yield. ^{1}H NMR (400 MHz, $CDCl_3$) δ (ppm): 1.66-1.8 (m, 12H), 3.3-3.47 (m, 2H), 6.90-7.80 (m, 16H). FTIR (Membrane, ν, cm^{-1}): 1778 (asym C=O, str), 1720 (sym C=O, str), 1349 (C-N, str), 831 (imide ring deformation). BET surface area = 565 m^2 g^{-1}, total pore volume = 0.39 cm^3 g^{-1} at (p/p_o = 0.98, adsorption). TGA analysis: (Nitrogen), initial weight loss due to thermal degradation commences at T_d = 500 °C.

Synthesis of TPDA-DAR polyimide

Into a dry 10 mL Schlenk tube were added the diaminoresorcinol (0.079 g, 0.4 mmol), triptycene dianhydride (0.28 g, 0.4 mmol), benzoic acid (0.29 g), freshly distilled *m*-cresol (2 ml) and triethylamine (0.11 ml). After stirring for a few minutes at room temperature and under a flow of nitrogen, the temperature was raised gradually to 80 °C and the mixture was then stirred at this temperature for 30 minutes. Thereafter, the temperature was raised gradually to 200 °C and maintained at that temperature for 2 hours. After cooling, the reaction mixture was precipitated in methanol. The resulting polymer was collected by filtration and purified by reprecipitation from DMAc into methanol-THF (50:50 v/v) and then dried under vacuum at 130 °C for 20 h to give a yellow powder in quantitative yield. ^{1}H NMR (400MHz, DMSO-d_6) δ (ppm): 1.76 (br m, 12H), 3.33-3.38 (m, 2H), 6.97-7.80 (m, 14H), 10.11 (br s, 2H). FTIR (Membrane, ν, cm^{-1}): 1776 (asym C=O, str), 1716 (sym C=O, str), 1355 (C-N, str), 825 (imide ring deformation), 3309 (OH stretching). BET surface area = 308 m^2 g^{-1}, total pore volume = 0.23 cm^3 g^{-1} at (p/p_o = 0.98, adsorption). TGA analysis: (Nitrogen), initial weight loss due to thermal degradation commences at T_d = 450 °C.

Characterization of the polymers

^{1}H NMR (400 MHz) was recorded on a Bruker DRX 400 spectrometer in a suitable solvent using tetramethylsilane as the internal standard. Chemical shifts (δ) are reported in ppm. Column chromatography was performed on silica gel 60A. Fourier transform infrared (FTIR) measurements were carried out using a Varian 670-IR FTIR spectrometer. Gel permeation chromatography (GPC, Viscotek) was conducted using chloroform as an eluent for TPDA-

*m*PDA only. GPC tests could not be performed on TPDA-DAR due to solubility limitations. Thermogravimetric analysis (TGA, TA Q-5000) measurements were performed under nitrogen atmosphere. All TGA runs entailed a drying step at 100 °C for 30 minutes followed by a temperature ramp of 3 °C/min up to 800 °C. The BET surface area of the polymers was determined by N_2 sorption at -196 °C using a Micromeritics ASAP 2020. Powder polymer samples were degassed under high vacuum at 150 °C for 24 hours prior to analysis. Analysis of the pore size distributions was performed using the NLDFT (Non-local density functional theory) model using N_2 at -196 °C sorption isotherms for carbon slit pore geometry provided by ASAP 2020 version 4.02 software.

Polymer film preparation

Solutions of TPDA-*m*PDA in chloroform (5 wt/vol%) and TPDA-DAR in DMAc were filtered through 0.45 μm polypropylene filters and isotropic films were obtained by very slow evaporation of the solvents at room temperature from a levelled and covered glass Petri dish. To remove any traces of residual solvent, the dry membranes were soaked in methanol for 24 h, air-dried, and then post-dried at 120 °C in a vacuum oven for 24 h. Complete casting solvent removal was confirmed by TGA measurements. The resulting tough and mechanically strong films (Fig. S1) with thickness of 40 ± 5 μm were used for gas permeability measurements. Film thickness and effective areas for gas permeation measurement were determined by a digital micrometer and scanner, respectively.

Fluorescence spectroscopy

Fluorescence excitation (excited at 400 nm) and emission spectra were collected against wavelength for dense polymer films (~45 μm) on a PerkinElmer LS45 setup in a 90° arrangement with fixed 10 nm slits. These measurements were conducted to investigate potential interchain charge transfer complex (CTC) formation of the hydroxyl-functionalized TPDA-DAR polyimide in the solid state.

Physisorption measurement

Nitrogen (-196 °C) sorption measurements were performed up to 1 atm using a Micromeritics ASAP 2020 apparatus equipped with a micropore upgrade. The BET surface area was obtained

from the N_2 isotherm over relative pressures $0.1 < p/p_o < 1$, where p_0=1 atm is the saturation pressure for N_2 and p is the gas pressure. Maximum pore volumes were identified at $p/p_0 < 0.99$ of the N_2 isotherm. NLDFT (non-local density functional theory) analysis of the N_2 isotherms for pore size distributions permits *qualitative* assessments of changes to the microporous texture that occur upon hydroxyl functionalization of TPDA-*m*PDA to TPDA-DAR [51].

Pure-gas permeation measurements

The pure-gas permeation measurements were conducted with a custom-designed permeation system using the constant-volume/variable-pressure method. The permeability was calculated from the steady-state rate of increase in pressure of the gas (*dp/dt*) in the permeate reservoir using the following equation:

$$P = \frac{VL}{ARTp_{up}} \times \frac{dp}{dt} \times 10^{10}$$

where *P* is the permeability coefficient in Barrers (1 Barrer=10^{-10} cm^3(STP) cm/cm^2 s cmHg), *V* the volume of the downstream gas reservoir, *L* the membrane thickness, *A* the membrane area, *R* the gas constant (0.278 cm^3 cmHg/(cm^3(STP) K), *T* the operating temperature and p_{up} the upstream pressure. The pure-gas permeability of He, H_2, N_2, O_2, CH_4, and CO_2 was measured at 35 °C and 2 atm. The pressure-dependence of CO_2 and CH_4 permeability was determined from 2 to 20 atm.

Mixed-gas permeation measurements

The mixed-gas permeation measurements of TPDA-*m*PDA and TPDA-DAR were performed at 35 °C using a custom-designed mixed-gas permeation system similar to that described by O'Brien et al. [52]. The feed gas mixture contained 50 vol.% CH_4 and 50 vol.% CO_2 and the total pressure was varied between 4 and 40 atm. The stage cut, that is, the permeate flow rate to feed flow rate, was set at 0.01. Under these conditions, the residue composition was essentially equal to that of the feed gas. CO_2 and CH_4 permeate concentrations were detected with a gas chromatograph (Agilent 3000A Micro GC) equipped with a thermal conductivity detector. The mixed-gas permeability was calculated by:

$$P_{CH_4} = 10^{10} \frac{y_{CH_4} V_d L}{x_{CH_4} p_{up} ART} \frac{dp}{dt}$$

$$P_{CO_2} = 10^{10} \frac{y_{CO_2} V_d L}{x_{CO_2} p_{up} ART} \frac{dp}{dt}$$

where *y* and *x* are the mole fractions in the permeate and feed respectively.

The CO_2/CH_4 selectivity was obtained from:

$$\alpha_{CO_2/CH_4} = \frac{y_{CO_2}/y_{CH_4}}{x_{CO_2}/x_{CH_4}}$$

Results and discussion

The physical properties of TPDA-*m*PDA and TPDA-DAR are listed in **Table 1**. TPDA-*m*PDA had a high molecular weight Mw of 209300 g mol^{-1} as determined by GPC in chloroform; the molecular weight of TPDA-DAR could not be determined as the polymer was only soluble in aprotic solvents such as DMAc, which were not compatible with our GPC instrument.

Table 1. Physical properties of TPDA-*m*PDA and TPDA-DAR polyimides.

Polymer	BET (m^2/g)	M_n (g/mol)	M_w (g/mol)	PDI	T_d (^oC)	Max pore volume** (cm^3/g)
TPDA-*m*PDA	565	129300	209300	1.62	500	0.39
TPDA-DAR	308	*	*	*	450	0.23

*GPC test could not be be performed due to solubility limitation in GPC solvent (chloroform).
** Determined by nitrogen adsorption at $p/p_0 = 0.99$.

The thermal stability of TPDA-*m*PDA and TPDA-DAR was determined by thermal gravimetric analysis, as shown in **Fig. 1**. The two polymers were thermally very stable with onset decomposition temperatures of 450 and 500 °C for TPDA-DAR and TPDA-*m*PDA, respectively.

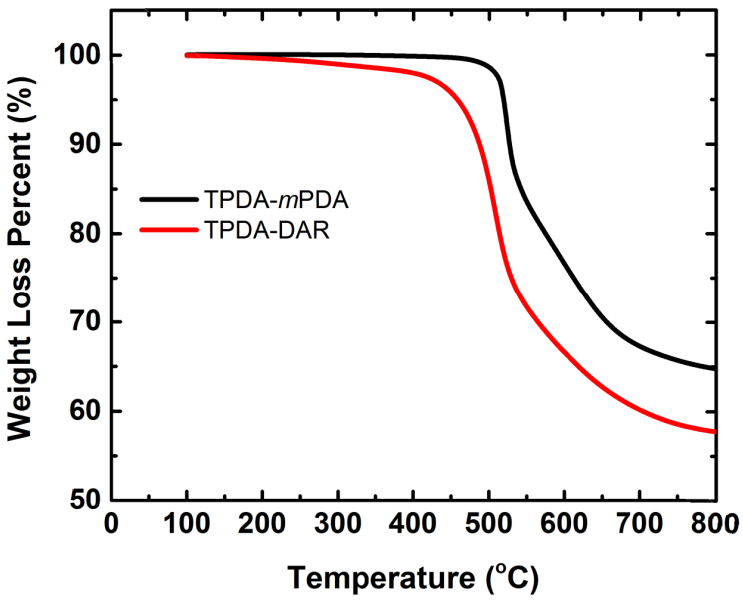

Fig. 1. Thermogravimetric analysis of TPDA-*m*PDA and TPDA-DAR polyimides.

CTC formation in hydroxyl-functionalized TPDA-DAR polyimide was identified via a peak in the intensity of the emission spectra collected by fluorescence spectroscopy. **Fig. 2** shows the emission spectra (400 nm excitation) for TPDA-*m*PDA and TPDA-DAR films. For dihydroxyl-functionalized TPDA-DAR a strong intensity peak was observed at 607 nm, clearly indicating CTC formation, which is typically formed between the nucleophilic five-member rings and electrophilic six-member rings in polyimides [42, 53-56]. The fluorescence intensity of the TPDA-*m*PDA polyimide showed essentially no indication of CTC formation, as shown in **Fig. 2**.

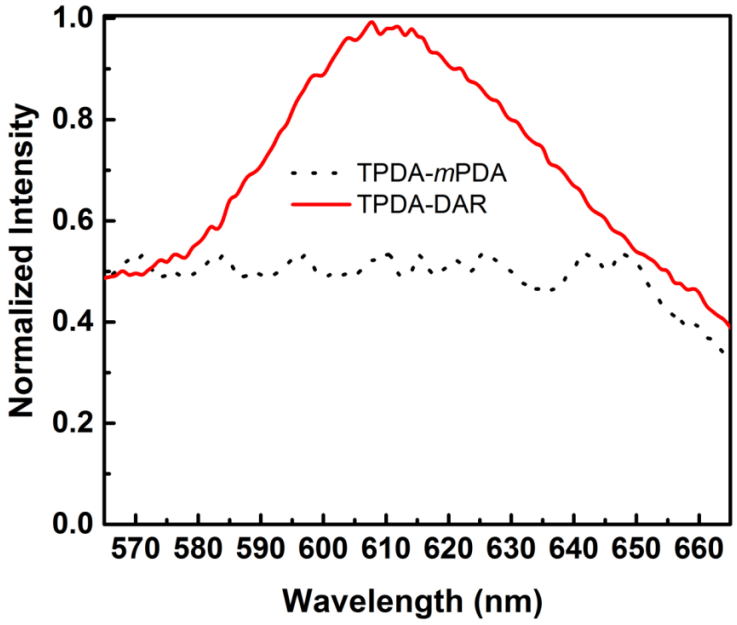

Fig. 2. Solid-state fluorescence emission spectra (excitation at 400 nm) of TPDA-*m*PDA and TPDA-DAR polyimides.

The influence of the dihydroxyl-functionalization on the microporosity of TPDA-DAR relative to that of TPDA-*m*PDA was assessed from N_2 physisorption isotherms (**Fig. 3**). The corresponding NLDFT-derived pore size distribution (PSD) based on N_2 adsorption is shown in **Fig. 4**. The introduction of hydroxyl groups in the polymer backbone decreased the BET surface area from 565 $m^{2/}g$ for TPDA-*m*PDA to 308 m^2/g for TPDA-DAR which was expected due the creation of CTCs between polymer chains leading to tightening of the entire polymer matrix and loss of free volume. Furthermore, NLDFT-derived pore size distributions from N_2 sorption isotherms indicate a larger *qualitative* shift of ultramicroporosity (pore size < 7 Å) in hydroxyl-functionalized TPDA-DAR towards smaller pores compared to TPDA-*m*PDA, as shown in **Fig. 4**. This result has significant implications on the differences in gas transport properties of the two polyimides, as discussed below.

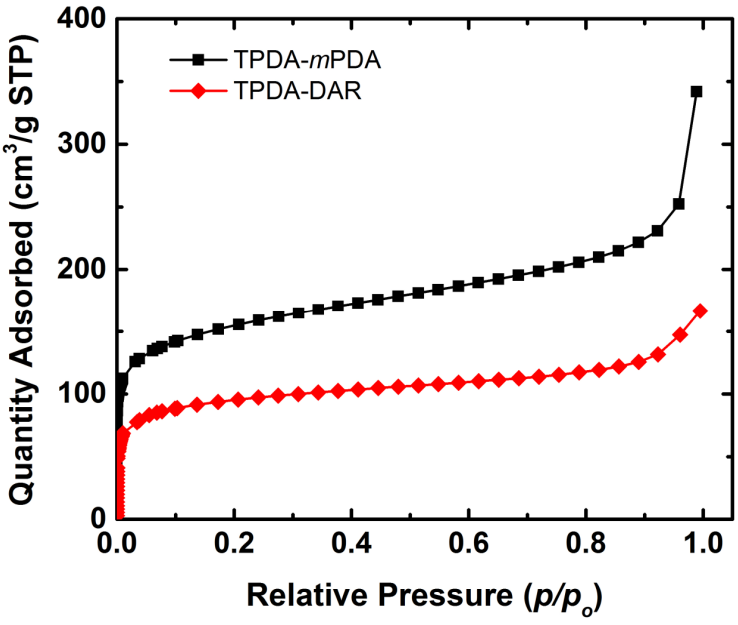

Fig. 3. Physisorption isotherms for TPDA-*m*PDA and TPDA-DAR using N_2 at -196 °C.

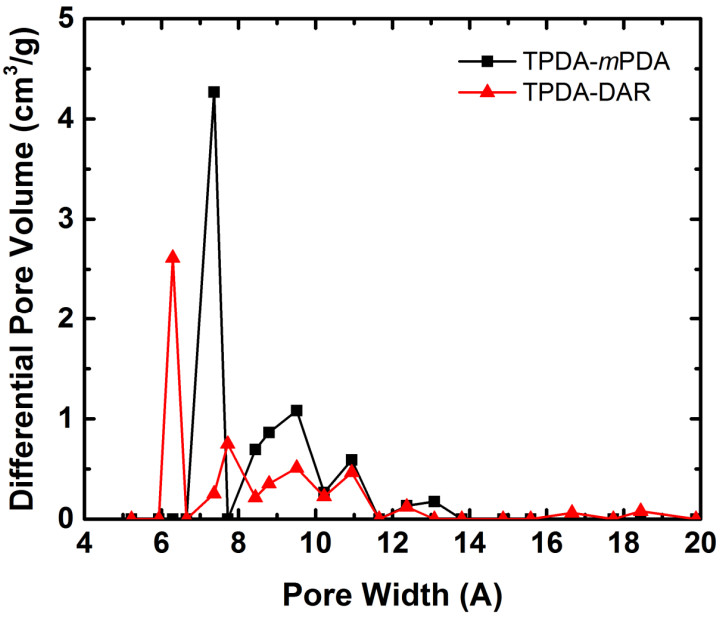

Fig. 4. NLDFT-based estimated pore size distribution obtained from N_2 isotherms for TPDA-*m*PDA and TPDA-DAR assuming carbon slit pore geometry.

Pure-gas permeation properties

To evaluate the gas transport properties of the TPDA-*m*PDA and TPDA-DAR polyimide membranes, pure-gas permeabilities of He, H_2, N_2, O_2, CH_4, and CO_2 were measured by the constant-volume/variable-pressure method. The permeability coefficient was calculated from the steady-state region of the permeate-pressure/time curve. The permeation data from this work in comparison to previously reported data for TPDA-APAF and cellulose triacetate, as an example of a commercial membrane material, are shown in **Table 2**. Owing to the microporosity introduced by the triptycene moiety and 9,10-diisopropyl-bridgehead substitution, the OH-functionalized TPDA-DAR polyimide was *significantly* more permeable than cellulose triacetate which is used in commercial membrane systems for CO_2/CH_4 separation. The CO_2 permeability of TPDA-DAR of 215 Barrer was about *30-fold* higher than of cellulose triacetate [57]. In addition, TPDA-DAR had a 2-fold higher CO_2 permeability and 20% higher CO_2/CH_4 selectivity compared to a related TPDA-APAF polyimide.

Table 2. Pure-gas permeabilities and ideal selectivities for TPDA-*m*PDA and TPDA-DAR polyimides.

Polymer	**Pure-gas permeability** (Barrer)						**Ideal selectivity** (α)		
	He	**H_2**	**N_2**	**O_2**	**CH_4**	**CO_2**	**CO_2/CH_4**	**H_2/CH_4**	**O_2/N_2**
TPDA-*m*PDA	251	431	13	65	11	349	32	39	5.0
TPDA-DAR	216	330	5.4	32	4.65	215	46	71	5.9
TPDA-APAF [53]	-	-	-	-	2.6	99	38	-	-
CTA [57]	19.6	15.5	0.23	1.46	0.20	6.6	33	78	6.3

TPDA-*m*PDA was more permeable than TPDA-DAR for all gases tested (**Table 2**) because of its larger surface area that is favorable for improving diffusivity as well as the absence of hydroxyl groups which reduced chain interactions due lack of CTC formation. The data clearly show that introducing hydroxyl functionality to the TPDA-based polyimide leads to a notable increase in selectivity (i.e CO_2/CH_4 selectivity was enhanced from 32 for non-hydroxyl functionalized TPDA-*m*PDA to 46 for TPDA-DAR with two hydroxyl groups in the diamine moiety. This 44% increase in selectivity was due to the existence of charge transfer complex formation between polymer chains that tighten the polymer structure, as previously reported for related polyimides

[42, 58]. As expected, the increase in selectivity was coupled with a 38% decrease in CO_2 permeability from 349 barrers to 215 barrers. This result is qualitatively consistent with the BET and PSD results discussed above. The gas permeabilities decrease in the order: $H_2>CO_2>O_2>N_2>CH_4$ which follows the order of kinetic diameters of the gases. A similar sequence was also reported for PIM-EA-TB, KAUST-PI-1 and 6FDA-DAT, which all contain bridged-bicyclic moieties with the same kink angles [59, 60].

The introduction of hydroxyl-functionalization to polyimides of intrinsic microporosity had also a clear effect on diffusion and solubility coefficients as well as diffusion and solubility selectivities, as shown in **Tables 3 and 4**. For example, the diffusion coefficients of CO_2 and CH_4 for TPDA-DAR decreased by 24% and 44%, respectively, relative to TPDA-*m*PDA, when two hydroxyl groups were introduced into the polymer repeat unit. Gas solubility in a membrane material is determined by its affinity to the gas molecules in addition to its surface area [43]. Introducing pendent polar OH groups can enhance the affinity of the polymers to CO_2 molecules due to the dipole of the C=O bonds. The solubility coefficient of carbon dioxide in dihydroxyl-functionalized TPDA-DAR was 12% higher than that of TPDA-*m*PDA. This finding is in agreement with previous work, which showed that the introduction of hydroxyl groups into 6FDA-based polyimide membranes increased the solubility of CO_2 [42, 53]. More importantly, however, is the decrease in diffusion coefficients and increase in diffusion selectivity in the TPDA-DAR polyimide due to hydroxyl functionalization; for example, the CO_2 diffusion coefficient decreased by 45% from 6.95 to 3.84 x 10^{-8} cm^2 s^{-1}. On the other hand, the CO_2/CH_4 diffusion selectivity increased by 38%, which led to an increase in the CO_2/CH_4 permselectivity from 32 for the TPDA-*m*PDA to 46 for TPDA-DAR polyimide.

Table 3. Pure-gas diffusion and solubility coefficients of N_2, O_2, CH_4 and CO_2 for TPDA-*m*PDA and TPDA-DAR polyimides.

	Diffusion coefficient (10^{-8} cm^2/s)				**Solubility coefficient** (10^{-2} $cm^3(STP)/(cm^3$ $cmHg)$)			
Polymer	N_2	O_2	CH_4	CO_2	N_2	O_2	CH_4	CO_2
TPDA-*m*PDA	4.2	19	1.1	6.95	3.1	3.4	9.9	50
TPDA-DAR	1.50	8.2	0.44	3.84	3.6	3.9	10.65	56

Table 4. Diffusion selectivities and solubility selectivities for TPDA-*m*PDA and TPDA-DAR polyimides.

	Diffusion selectivity $(\alpha)_D$		**Solubility selectivity** $(\alpha)_S$	
Polymer	O_2/N_2	CO_2/CH_4	O_2/N_2	CO_2/CH_4
TPDA-*m*PDA	4.52	6.32	1.1	5.05
TPDA–DAR	5.47	8.73	1.08	5.26

High-pressure mixed-gas CO_2/CH_4 permeation properties

Binary CO_2/CH_4 mixed-gas (1:1 molar mixture) permeation properties for TPDA-*m*PDA and TPDA-DAR polyimides were determined at a total feed pressure of 40 atm at 35 °C with increasing CO_2 partial pressures (2, 5, 10, 15 and 20 atm), and the effect of CO_2 partial pressure on CO_2/CH_4 selectivity was exploited. To determine any potential plasticization effects of the polyimides in the mixture experiments, pure-gas CO_2 and CH_4 permeabilities were also measured at 35 °C over a pressure range of 2-20 atm (**Fig. 5**). As expected for glassy polymers, the pure CO_2 permeability of both polyimides decreased continuously by increasing the feed pressure up to 20 atm due to dual-mode sorption behavior. This result indicates that CO_2-induced plasticization did not occur in the two polyimides up to 20 atm. The pure CH_4 permeability of TPDA-*m*PDA decreased slightly and that of TPDA-DAR was essentially constant up to 20 atm. Because the relative decrease in CO_2 permeability was larger than that of methane in the two polymers, their pure-gas CO_2/CH_4 selectivity decreased as a function of feed pressure, as shown in **Fig. 6**.

The CO_2 and CH_4 permeability isotherms of the TPDA-*m*PDA and TPDA-DAR polyimide membranes determined with a mixed-gas feed of 50 vol.% CH_4 and 50 vol.% CO_2 up to 40 atm are shown in **Fig. 7** and **Fig. 8**, respectively.

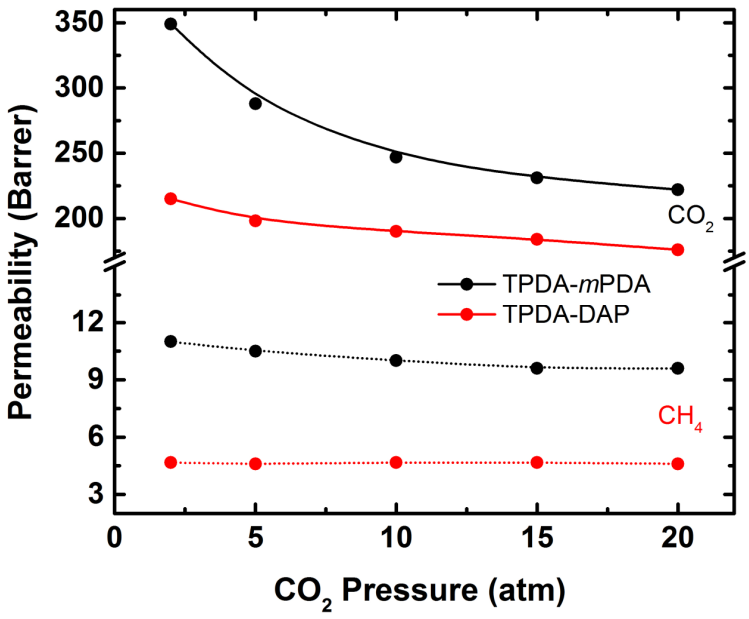

Fig. 5. Pressure dependence of pure-gas CO_2 and CH_4 permeability for TPDA-*m*PDA and TPDA-DAR polyimides at 35 °C.

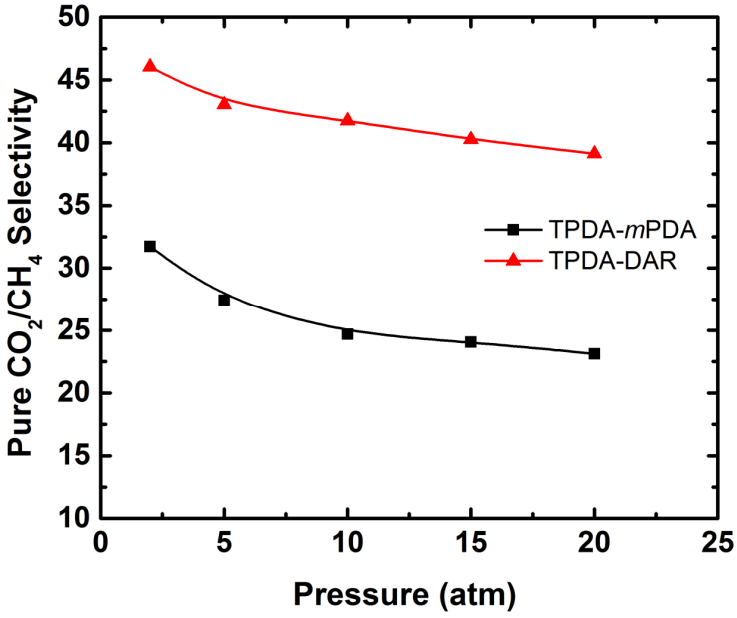

Fig. 6. Pressure dependence of pure-gas CO_2/CH_4 selectivity for TPDA-*m*PDA and TPDA-DAR polyimides at 35 °C.

The mixed-gas CO_2 permeabilities of both polymers were lower than those determined with pure CO_2 at the same partial pressures, as shown in **Fig. 7** and **Fig. 8**. This phenomenon is usually attributed to competitive sorption between CO_2 and CH_4 in the polymer matrix and has been previously observed for several polyimides of intrinsic microporosity [61, 62]. The mixed- and pure-gas CH_4 permeabilities of TPDA-*m*PDA were similar; however the mixed-gas permeability increased slightly by ~10% with feed pressure, potentially indicating the onset of plasticization around 15-20 atm CO_2 partial pressure. On the other hand, the mixed-gas CH_4 permeability of TPDA-DAR was lower across the whole pressure range and essentially independent of feed pressure.

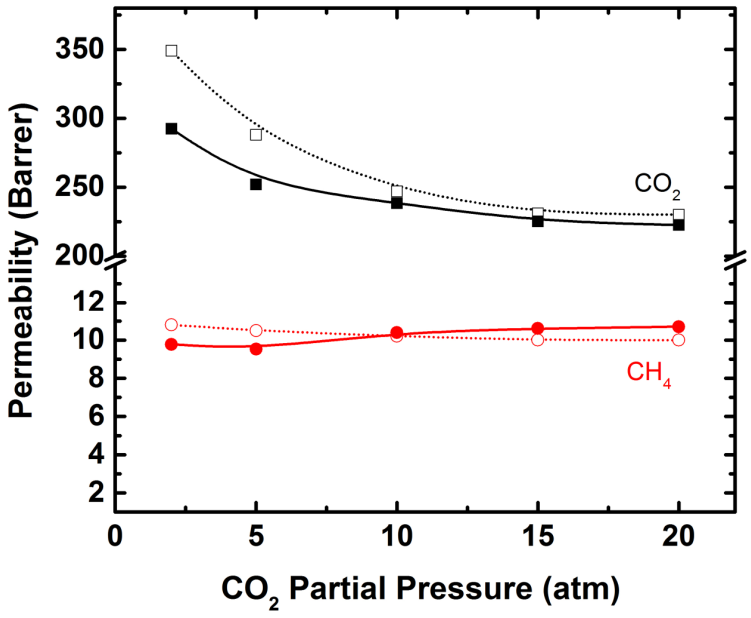

Fig. 7. Pressure-dependence of pure and mixed-gas CH_4 and CO_2 permeabilities for TPDA-*m*PDA polyimide (50:50 CO_2:CH_4 mixture; 35 ^oC). Lines are drawn to guide the eye. Open points: pure-gas; closed points: mixed-gas.

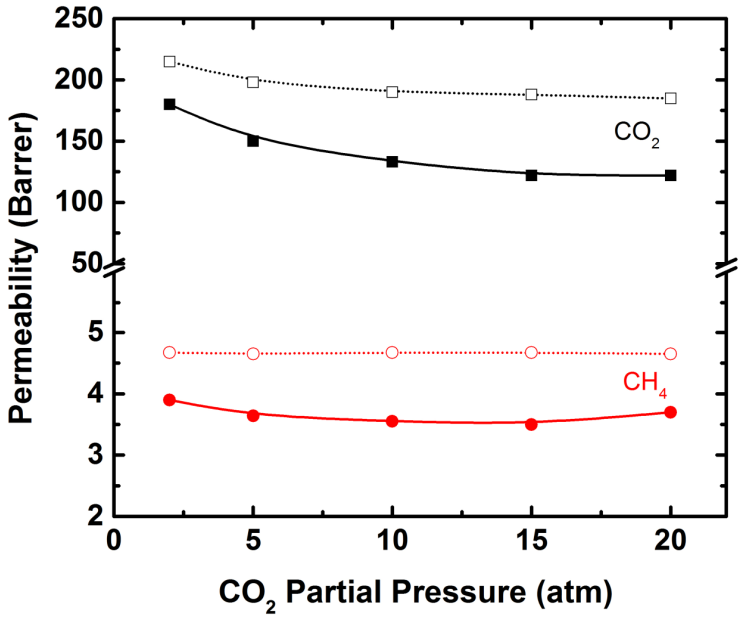

Fig. 8. Pressure-dependence of pure and mixed-gas CH_4 and CO_2 permeabilities for TPDA-DAR polyimide (50:50 CO_2:CH_4 mixture; 35 ^oC). Lines are drawn to guide the eye. Open points: pure-gas; closed points: mixed-gas.

The mixed-gas CO_2/CH_4 selectivity was lower than that determined under pure-gas permeation conditions for both polymers, as shown in **Fig. 9**. This behavior is commonly observed for microporous glassy polymers, including polyimides [46, 48, 60]. The lower mixed-gas CO_2/CH_4 selectivity resulted from the aforementioned competitive sorption behavior of the polyimides. Nevertheless, the mixed-gas permeation properties of the dihydroxyl-functionalized TPDA-DAR polyimide exhibited promising gas separation properties with a CO_2 permeability of 140 Barrer and CO_2/CH_4 selectivity of 38 at a partial CO_2 pressure of 10 atm.

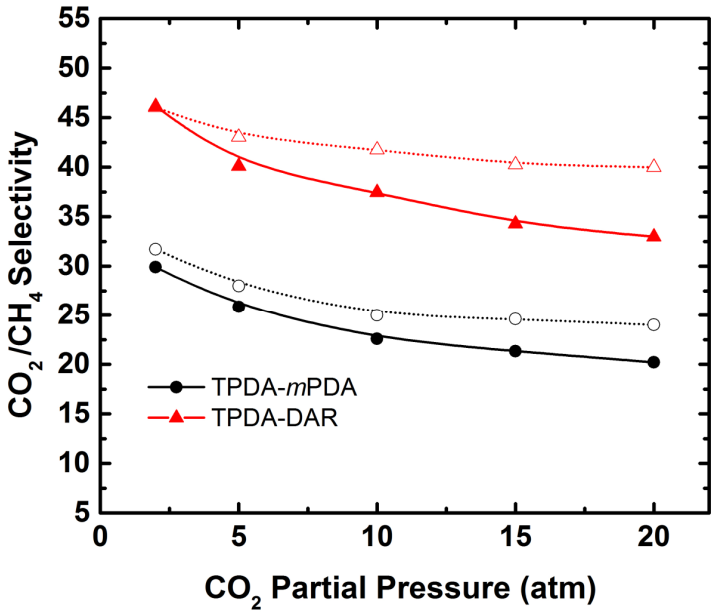

Fig. 9. Pressure-dependence of pure and mixed-gas CO_2/CH_4 selectivities for TPDA-*m*PDA and TPDA-DAR polyimides (50:50 CO_2:CH_4 mixture, 35 ^oC). Lines are drawn to guide the eye. Open points: pure-gas; closed points: mixed-gas.

Conclusions

In this work, a dihydroxyl-functionalized triptycene-based polyimide of intrinsic microporosity (TPDA-DAR) was developed and its pure- and mixed-gas permeation properties were compared to those of a related triptycene polyimide without functional OH-groups in the repeat unit (TPDA-*m*PDA). The two polymers showed good solubility, processability, high thermal stability and promising gas separation performance. The OH-functionalized TPDA-DAR exhibited significantly higher gas permeability than other reported hydroxyl-functionalized polyimides. In addition, TPDA-DAR showed higher CO_2/CH_4 selectivity than previously reported PIMs and exhibited excellent plasticization resistance as compared to many previously reported polyimides, as demonstrated by its high CO_2/CH_4 selectivity of 38 under mixed-gas conditions at 10 atm partial feed pressure. Based on our high-pressure binary mixed-gas permeation data, hydroxyl-functionalized polyimides are excellent candidate materials for development of asymmetric or thin-film composite membranes for industrial natural gas sweetening. However, future work needs to address the effect of condensable natural gas feed components, such as H_2S,

H_2O, aromatics etc. on the plasticization resistance of OH-containing polyimides, as previously suggested by Wind et al. [37].

Acknowledgments

The research reported in this publication was supported by funding from King Abdullah University of Science and Technology (KAUST).

References

1. Peters L, Hussain A, Follmann M, Melin T, and Hagg MB. Chemical Engineering Journal 2011;172(2-3):952-960.
2. Bernardo P, Drioli E, and Golemme G. Industrial & Engineering Chemistry Research 2009;48(10):4638-4663.
3. Baker RW and Lokhandwala K. Industrial & Engineering Chemistry Research 2008;47(7):2109-2121.
4. Kidnay AJ and Parrish WR. Fundamentals of natural gas processing: CRC Press, 2006.
5. Baker RW. Industrial & Engineering Chemistry Research 2002;41(6):1393-1411.
6. Koros WJ and Mahajan R. Journal of Membrane Science 2001;181(1):141-141.
7. Henis JMS and Tripodi MK. Science 1983;220(4592):11-17.
8. Bessarabov D, Cheryan M, Fane A, Franken A, Gobina E, Merry A, Nyström M, Pabby A, Pearce G, and Pfromm P. Membrane Technology 2010;2010:2.
9. Carta M, Malpass-Evans R, Croad M, Rogan Y, Jansen JC, Bernardo P, Bazzarelli F, and McKeown NB. Science 2013;339(6117):303-307.
10. Carta M, Croad M, Malpass-Evans R, Jansen JC, Bernardo P, Clarizia G, Friess K, Lanč M, and McKeown NB. Advanced Materials 2014;26(21):3526-3531.
11. Rogan Y, Malpass-Evans R, Carta M, Lee M, Jansen JC, Bernardo P, Clarizia G, Tocci E, Friess K, and Lanč M. Journal of Materials Chemistry A 2014;2(14):4874-4877.
12. Freeman B and Pinnau I. Polymeric materials for gas separations, in Polymer Membranes for Gas and Vapor Separation, B. D. Freeman, I. Pinnau (Eds.), ACS Symposium Series Vol. 733, 1999, pp. 1-27.
13. Koros W and Fleming G. Journal of Membrane Science 1993;83(1):1-80.

14. Budd PM, Ghanem BS, Makhseed S, McKeown NB, Msayib KJ, and Tattershall CE. Chemical Communications 2004(2):230-231.
15. Budd PM, Elabas ES, Ghanem BS, Makhseed S, McKeown NB, Msayib KJ, Tattershall CE, and Wang D. Advanced Materials 2004;16(5):456-459.
16. McKeown NB and Budd PM. Chemical Society Reviews 2006;35(8):675-683.
17. Budd PM, Msayib KJ, Tattershall CE, Ghanem BS, Reynolds KJ, McKeown NB, and Fritsch D. Journal of Membrane Science 2005;251(1):263-269.
18. Budd PM, McKeown NB, Ghanem BS, Msayib KJ, Fritsch D, Starannikova L, Belov N, Sanfirova O, Yampolskii Y, and Shantarovich V. Journal of Membrane Science 2008;325(2):851-860.
19. Du N, Robertson GP, Pinnau I, and Guiver MD. Macromolecules 2009;42(16):6023-6030.
20. Du N, Robertson GP, Pinnau I, and Guiver MD. Macromolecules 2010;43(20):8580-8587.
21. Du N, Robertson GP, Song J, Pinnau I, Thomas S, and Guiver MD. Macromolecules 2008;41(24):9656-9662.
22. Ghanem BS, McKeown NB, Budd PM, Selbie JD, and Fritsch D. Advanced Materials 2008;20(14):2766-2771.
23. Ghanem BS, McKeown NB, Budd PM, and Fritsch D. Macromolecules 2008;41(5):1640-1646.
24. Carta M, Msayib KJ, Budd PM, and McKeown NB. Org. Lett. 2008;10(13):2641-2643.
25. Short R, Carta M, Bezzu CG, Fritsch D, Kariuki BM, and McKeown NB. Chemical Communications 2011;47(24):6822-6824.
26. Du N, Park HB, Robertson GP, Dal-Cin MM, Visser T, Scoles L, and Guiver MD. Nature Materials 2011;10(5):372-375.
27. Du N, Robertson GP, Pinnau I, Thomas S, and Guiver MD. Macromolecular Rapid Communications 2009;30(8):584-588.
28. Du N, Robertson GP, Song J, Pinnau I, and Guiver MD. Macromolecules 2009;42(16):6038-6043.
29. Mason CR, Maynard-Atem L, Al-Harbi NM, Budd PM, Bernardo P, Bazzarelli F, Clarizia G, and Jansen JC. Macromolecules 2011;44(16):6471-6479.

30. Swaidan R, Ghanem BS, Litwiller E, and Pinnau I. Journal of Membrane Science 2014;457:95-102.
31. Song Q, Cao S, Pritchard RH, Ghalei B, Al-Muhtaseb SA, Terentjev EM, Cheetham AK, and Sivaniah E. Nature Communications 2014;5.
32. Kim T-H, Koros WJ, and Husk GR. Separation Science and Technology 1988;23(12-13):1611-1626.
33. Stern SA. Journal of Membrane Science 1994;94(1):1-65.
34. Liaw D-J, Wang K-L, Huang Y-C, Lee K-R, Lai J-Y, and Ha C-S. Progress in Polymer Science 2012;37(7):907-974.
35. White LS, Blinka TA, Kloczewski HA, and Wang I-f. Journal of Membrane Science 1995;103(1):73-82.
36. Ayala D, Lozano AE, de Abajo J, Garcia-Perez C, de la Campa JG, Peinemann KV, Freeman BD, and Prabhakar R. Journal of Membrane Science 2003;215(1-2):61-73.
37. Wind JD, Paul DR, and Koros WJ. Journal of Membrane Science 2004;228(2):227-236.
38. Houde AY, Kawakami H, Stern SA, and Zhou G. Material and process for separating carbon dioxide from methane. US Patent 5,591,250, 1997.
39. Ma X, Swaidan R, Belmabkhout Y, Zhu Y, Litwiller E, Jouiad M, Pinnau I, and Han Y. Macromolecules 2012;45(9):3841-3849.
40. Park SH, Kim KJ, So WW, Moon SJ, and Lee SB. Macromolecular Research 2003;11(3):157-162.
41. Kim KJ, Park SH, So WW, Ahn DJ, and Moon SJ. Journal of Membrane Science 2003;211(1):41-49.
42. Alaslai N, Ghanem B, Alghunaimi F, Litwiller E, and Pinnau I. Journal of Membrane Science 2016;505:100-107.
43. Jung CH and Lee YM. Macromolecular Research 2008;16(6):555-560.
44. Comesaña-Gándara B, Hernández A, Jose G, de Abajo J, Lozano AE, and Lee YM. Journal of Membrane Science 2015;493:329-339.
45. Ghanem BS, McKeown NB, Budd PM, Al-Harbi NM, Fritsch D, Heinrich K, Starannikova L, Tokarev A, and Yampolskii Y. Macromolecules 2009;42(20):7881-7888.
46. Swaidan R, Ghanem B, Al-Saeedi M, Litwiller E, and Pinnau I. Macromolecules 2014;47(21):7453-7462.

47. Ghanem BS, Swaidan R, Litwiller E, and Pinnau I. Advanced Materials 2014;26(22):3688-3692.
48. Swaidan R, Al-Saeedi M, Ghanem B, Litwiller E, and Pinnau I. Macromolecules 2014;47(15):5104-5114.
49. Swaidan R, Ghanem B, and Pinnau I. ACS Macro Letters 2015;4(9):947-951.
50. Robeson LM. Journal of Membrane Science 2008;320(1-2):390-400.
51. Jeromenok J and Weber J. Langmuir 2013;29(42):12982-12989.
52. O'Brien KC, Koros WJ, Barbari TA, and Sanders ES. Journal of Membrane Science 1986;29(3):229-238.
53. Swaidan R, Ghanem B, Litwiller E, and Pinnau I. Journal of Membrane Science 2015;475:571-581.
54. Duthie X, Kentish S, Pas SJ, Hill AJ, Powell C, Nagai K, Stevens G, and Qiao G. Journal of Polymer Science Part B-Polymer Physics 2008;46(18):1879-1890.
55. Kawakami H, Mikawa M, and Nagaoka S. Journal of Membrane Science 1996;118(2):223-230.
56. Wachsman ED and Frank CW. Polymer 1988;29(7):1191-1197.
57. Puleo AC, Paul DR, and Kelley SS. Journal of Membrane Science 1989;47(3):301-332.
58. Swaidan R, Ghanem B, Litwiller E, and Pinnau I. Journal of Membrane Science 2015;475:571-581.
59. Carta M, Malpass-Evans R, Croad M, Rogan Y, Lee M, Rose I, and McKeown NB. Polymer Chemistry 2014;5(18):5267-5272.
60. Alghunaimi F, Ghanem B, Alaslai N, Swaidan R, Litwiller E, and Pinnau I. Journal of Membrane Science 2015;490:321-327.
61. Vieth W, Howell J, and Hsieh J. Journal of Membrane Science 1976;1:177-220.
62. Koros W, Chern R, Stannett V, and Hopfenberg H. Journal of Polymer Science: Polymer Physics Edition 1981;19(10):1513-1530.

Highlights

- A hydroxyl-functionalized microporous polyimide TPDA-DAR was synthesized and characterized.
- OH-functionalized TPDA-DAR polyimide showed high pure-gas CO_2/CH_4 selectivity (46 at 2 atm).
- Mixed-gas CO_2/CH_4 selectivity at 10 atm partial CO_2 pressure was reduced to 38.
- Plasticization was mitigated by introduction of OH groups at least up to 10 atm partial CO_2 pressure.